A new stochastic cellular automaton model on traffic flow and its jamming phase transition

2006 J. Phys. A: Math. Gen. 39 15327

(http://iopscience.iop.org/0305-4470/39/50/002)

INSTITUTE OF PHYSICS PUBLISHING JOURNAL OF PHYSICS A: MATHEMATICAL AND GENERAL

J. Phys. A: Math. Gen. **39** (2006) 15327–15339 doi:10.1088/0305-4470/39/50/002

A new stochastic cellular automaton model on traffic flow and its jamming phase transition

Satoshi Sakai[1], **Katsuhiro Nishinari**[2] **and Shinji Iida**[1]

[1] Department of Applied Mathematics and Informatics, Ryukoku University, Shiga 520-2194, Japan
[2] Department of Aeronautics and Astronautics, Tokyo University, Tokyo 113-8656, Japan

Received 7 September 2006, in final form 25 October 2006
Published 30 November 2006
Online at stacks.iop.org/JPhysA/39/15327

Abstract

A general stochastic traffic cellular automaton (CA) model, which includes the slow-to-start effect and driver's perspective, is proposed in this paper. It is shown that this model includes well-known traffic CA models such as the Nagel–Schreckenberg model, the quick-start model and the slow-to-start model as specific cases. Fundamental diagrams of this new model clearly show metastable states around the critical density even when the stochastic effect is present. We also obtain analytic expressions of the phase transition curve in phase diagrams by using approximate flow-density relations at boundaries. These phase transition curves are in excellent agreement with numerical results.

PACS numbers: 05.65.+b, 45.70.Vn

1. Introduction

A traffic jam is one of the most serious issues in modern society. In Japan, the amount of financial loss due to traffic jams approximates 12 thousand billion yen per year according to the Road Bureau, Ministry of Land, Infrastructure and Transport.

Recently, investigations towards understanding traffic jam formation are done not only by engineers but also actively by physicists [1]. The typical examples are developing realistic mathematical traffic models which give (with the help of numerical simulations) various phenomena that reproduce empirical traffic flow [2–8], fundamental studies of traffic models such as obtaining exact solutions, clarifying the structure of flow-density diagrams or phase diagrams [9–12], analysis of traffic flow with a bottleneck [13, 14] and studies of traffic flow in various road types [15–17].

We can classify microscopic traffic models into two kinds: optimal velocity models and cellular automaton (CA) models. A merit of using a CA model is that, owing to its discreteness, it can be expressed in relatively simple rules even in the case of complex road geometry. Thus numerical simulations can be effectively performed and various structures of roads with

multiple lanes can be easily incorporated into numerical simulations. However, the study of the traffic CA model has relatively short history and we have not yet obtained the 'best' traffic CA model which should be both realistic as well as simple. There are many traffic CA models proposed so far. For example, Rule-184 [18], which was originally presented by Wolfram as a part of elementary CA, is the simplest traffic model. The Fukui–Ishibashi (FI) model [5] takes into account the high speed effect of vehicles, Nagel–Schreckenberg (NS) model [2] deals with the random braking effect, quick-start (QS) model [6] with the driver's anticipation effect and the slow-to-start (SlS) model [3] with the inertia effect of cars. The asymmetric simple exclusion process (ASEP) [10], which is a simple case of the NS model, has been often used to describe general non-equilibrium systems in low dimensions. An extension of the NS model, called the VDR model, is considered by taking into account a kind of slow-to-start effect [1]. Recently Kerner *et al* proposed an elaborated CA model by taking into account the synchronized distance between cars [19]. Each of these models reproduces a part of features of empirical traffic flow.

A fundamental diagram is usually used to examine whether a model is practical or not by comparing empirical data (see figure 1) and simulation results. A fundamental diagram is called a flow-density graph in other words. And it chiefly consists of three parts: free-flow line, jamming line and metastable branches. On the free-flow line, flow increases with density, while on the jamming line flow decreases with density. The critical density divides the free-flow line from the jamming line. Around the critical density, close to the maximal flow, there appear some metastable branches. In general, the metastable branches are unstable states where cars can run like a free-flow state even if the density surpasses the critical density. The characteristics of individual fundamental diagrams for the above CA models are as follows: the fundamental diagram of Rule-184 has an isosceles triangular shape. The critical density in a FI model, which divides the whole region into free flow phase and jamming phase, is lower than that of Rule-184, and the maximal flow reaches a higher value due to the high speed effect. The critical density and maximal flow in a QS model are higher than those of Rule-184, because more than one car can move simultaneously. The maximal flow of the ASEP or NS model is lower than those of the Rule-184 or FI model because of the random braking effect. In the case of a SlS model, a fundamental diagram is significantly different from these models. Its fundamental diagram shows metastable branches near the critical density [3, 4]. Because metastable branches are clearly observed in a practical fundamental diagram (see figure 1), we think realistic traffic models should reproduce such branches. We note that the study of these metastable branches in the high flow region is very important for a plan of ITS (intelligent transport systems). The states in these branches are dangerous, because of the lack of headway between vehicles. On the other hand, they have the highest transportation efficiency because each vehicle's speed is very high regardless of the short headway.

In this paper, we propose a general stochastic traffic CA model which includes, as special cases, well-known models such as the NS model, QS model and SlS model. The paper is organized as follows. We first define our model in section 2. Next, fundamental diagrams, flow-α-β diagrams and phase diagrams of this new model will be presented in sections 3 and 4. Finally we show analytical expressions of phase transition curves in phase diagrams in section 5.

2. A new stochastic CA model

In 2004, a new deterministic traffic model which includes both slow-to-start effects and driver's perspective (anticipation) was presented by Nishinari, Fukui and Schadschneider [7]. We call

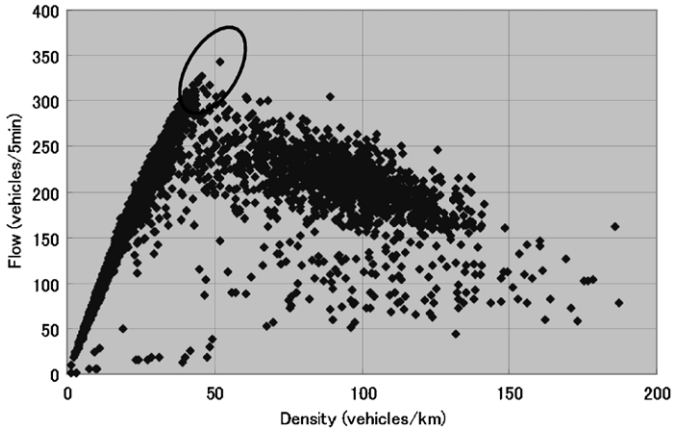

Figure 1. A fundamental diagram is plotted with the use of empirical data. These data were collected at the Tomei expressway in Japan by the Japan Highway Public Corporation. The road consists of two-lanes. Each point in the diagram corresponds to an average over a time interval of 5 min. The density is calculated from the flow divided by the average velocity. We can see metastable points which are inside the circle at the highest flux region of free flow.

this model the Nishinari–Fukui–Schadschneider (NFS) model. In this paper, we further extend the NFS model by incorporating stochastic effects.

First, the updating rules of the NFS model are written as

$$v_i^{(1)} = \min\left\{V_{\max}, v_i^{(0)} + 1\right\} \tag{1}$$

$$v_i^{(2)} = \min\left\{v_i^{(1)}, x_{i+S}^{t-1} - x_i^{t-1} - S\right\} \tag{2}$$

$$v_i^{(3)} = \min\left\{v_i^{(2)}, x_{i+S}^{t} - x_i^{t} - S\right\} \tag{3}$$

$$v_i^{(4)} = \min\left\{v_i^{(3)}, x_{i+1}^{t} - x_i^{t} - 1 + v_{i+1}^{(3)}\right\} \tag{4}$$

$$x_i^{t+1} = x_i^t + v_i^{(4)} \tag{5}$$

in Lagrange representation. In these rules, x_i^t is a Lagrange variable that denotes the position of the ith car at time t. $v_i^{(0)}$ is velocity $x_i^t - x_i^{t-1}$, and the parameter S represents the interaction horizon of drivers and is called an anticipation parameter. And we repeat and apply this rule again as $v_i^{(0)} \longleftarrow v_i^{(4)}$ in the next time. In this paper, we use a parallel update scheme where those rules are applied to all cars simultaneously. Rule (1) means acceleration and the maximum velocity is $V_{\max}$, (2) realizes the slow-to-start effect, (3) means deceleration due to other cars, (4) guarantees avoidance of collision. Cars are moved according to (5). The characteristic of the NFS model is the occurrence of a metastable branch in a fundamental diagram because of the slow-to-start effect. It should be noted that the slow-to-start rule adopted in this paper (2) is different from the previously proposed ones [4].

Next, we explain a stochastic extension of the NFS model. The model is described as follows:

$$v_i^{(1)} = \min\left\{V_{\max}, v_i^{(0)} + 1\right\} \tag{6}$$

$$v_i^{(2)} = \min\left\{v_i^{(1)}, x_{i+S}^{t-1} - x_i^{t-1} - S\right\} \qquad \text{with the probability } q \tag{7}$$

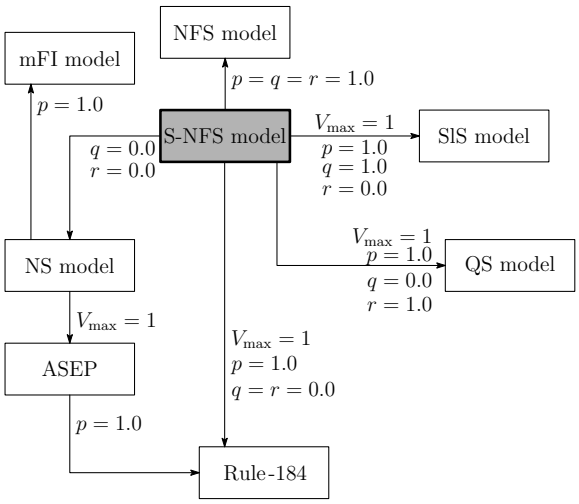

Figure 2. A reduction map of various traffic CA models.

$$v_i^{(3)} = \min\left\{v_i^{(2)}, x_{i+S}^t - x_i^t - S\right\} \tag{8}$$

$$v_i^{(4)} = \max\left\{0, v_i^{(3)} - 1\right\} \qquad \text{with the probability } 1 - p \tag{9}$$

$$v_i^{(5)} = \min\left\{v_i^{(4)}, x_{i+1}^t - x_i^t - 1 + v_{i+1}^{(4)}\right\} \tag{10}$$

$$x_i^{t+1} = x_i^t + v_i^{(5)}. \tag{11}$$

We define three independent parameters—p, q and r: the parameter p controls the random-braking effect; that is, a vehicle decreases its velocity by 1 with the probability $1 - p$. The parameter q denotes the probability that the slow-to-start effect is on; the rule (7) is effective with the probability q. r denotes the probability of anticipation; $S = 2$ with the probability r and $S = 1$ with $1 - r$, hence the average of S is $\langle S\rangle = 1 + r$. This value of S is used in rules (7) and (8). We note that in order to reproduce an empirical fundamental diagram the value of S should lie between $S = 1$ and $S = 2$ [7]. Thus we call this new extended model the stochastic(S)-NFS model. A remarkable point is that the S-NFS model includes most of the other models when parameters are chosen specifically (see figure 2). Here, the 'modified(m) FI model' means a modification of the original FI model so that the increase of car's velocity is at most unity per one time step, because, in the original model, cars can suddenly accelerate, for example, from velocity $v = 0$ to $v = V_{\max}$, which seems to be unrealistic.

3. Fundamental diagram

In this section, we consider fundamental diagrams of the S-NFS model on a periodic boundary condition (PBC). Figure 3 shows fundamental diagrams with the maximum speed $V_{\max} = 1$. The parameter sets (a), (c), (g) and (i) correspond to Rule-184, the SlS model, QS model with $S = 2$ and NFS model, respectively. Figure 4 shows those with maximum speed $V_{\max} = 3$. Case (a) is a mFI model with $V_{\max} = 3$ and (i) is a NFS model.

The following two points are worthwhile to be mentioned:

(1) Although free flow and jamming lines are both straight for $r = 0$ or $r = 1.0$, the shape of jamming lines is roundish for $r = 0.5$ (see figures 3(d) or 4(d), (e), (f)) like ASEP

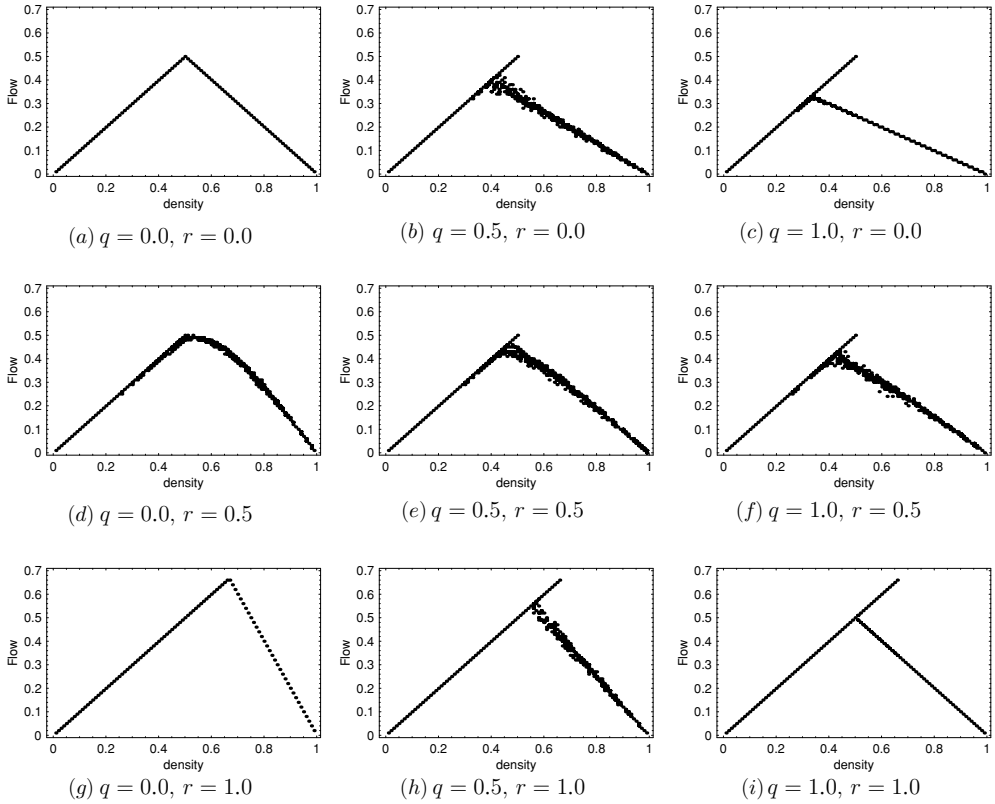

(*a*) $q = 0.0$, $r = 0.0$ (*b*) $q = 0.5$, $r = 0.0$ (*c*) $q = 1.0$, $r = 0.0$

(*d*) $q = 0.0$, $r = 0.5$ (*e*) $q = 0.5$, $r = 0.5$ (*f*) $q = 1.0$, $r = 0.5$

(*g*) $q = 0.0$, $r = 1.0$ (*h*) $q = 0.5$, $r = 1.0$ (*i*) $q = 1.0$, $r = 1.0$

Figure 3. Fundamental diagrams of the S-NFS model with $p = 1.0$, $L = 100$ and $V_{\max} = 1$. We repeat simulations for ten initial conditions at each density. The flow is averaged over the range from $t = 50$ to $t = 100$. When $q \neq 0$ and for uniform initial distributions, metastable branches are clearly seen.

with random braking effect ($p < 1.0$). The origin of this behaviour is as follows: two successive cars can move simultaneously as long as $S = 2$. However, once S of a car moving rear changes to 1, this car must stop. Hence the random change of S plays a similar role as random braking.

(2) As is seen in figure 4(h), metastable states 'stably' exist even in the presence of stochastic effects, although in many other models metastable states soon vanish due to any perturbations. There are also some new branches around the critical density in our model. As seen in figure 1, these new branches may be related to the wide scattering area around the density 60–125 (vehicles km^{-1}) in the observed data. Thus we believe we have successfully reproduced the metastable branches observed 'stably' in the empirical data.

4. Phase diagram

In this section, we consider phase diagrams of the S-NFS model with an open boundary condition (OBC) when $V_{\max} = 1$. Figure 5 shows our update rules for OBC:

(1) We put two cells at the sites -2, -1. At each site a car is injected with probability α. The car's velocity is set to 1.

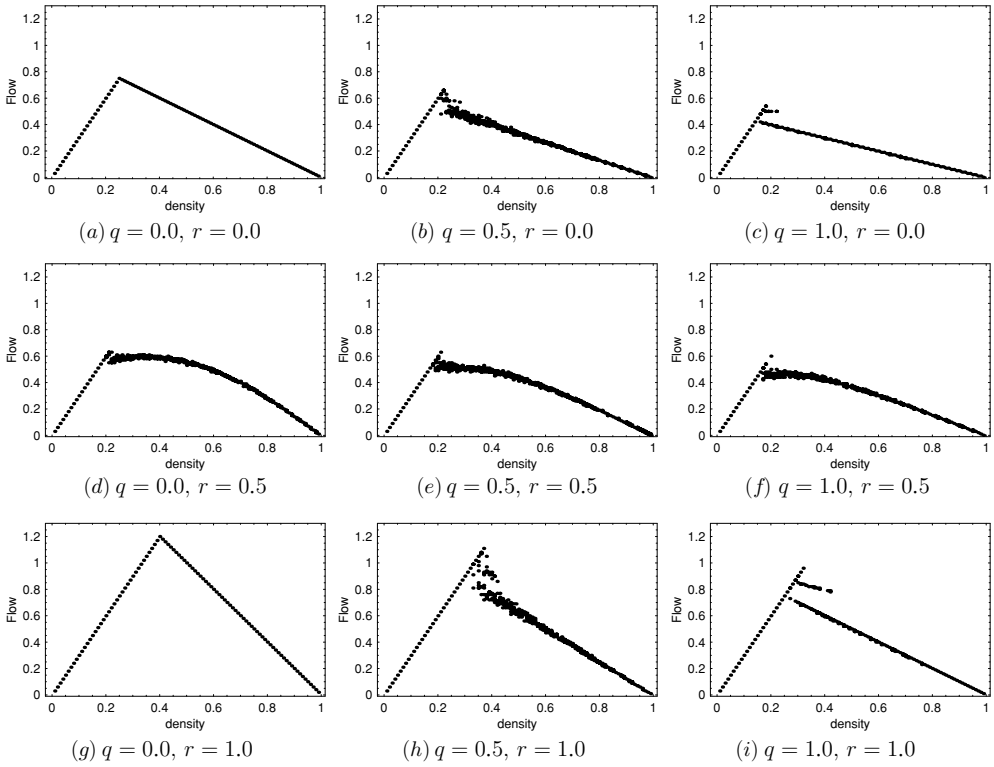

Figure 4. Fundamental diagrams of the S-NFS model with $p = 1.0$, $L = 100$ and $V_{\max} = 3$. Contrary to the cases with $V_{\max} = 1$, metastable states can remain even for random initial distributions.

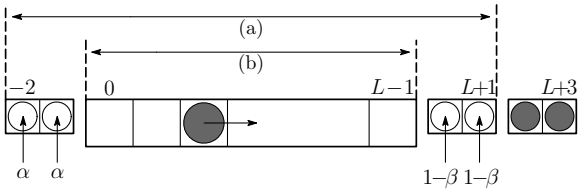

Figure 5. Updating rules for an open boundary condition of the S-NFS model when $V_{\max} = 1$. (*a*) Update rules (6)–(11) are applied to cars within this region. (*b*) The rule of slow-to-start (7) is effective only when $0 \leqslant x_i^{t-1}$ and $x_{i+S}^{t-1} \leqslant L - 1$.

(2) We put cells at the sites L, $L + 1$, and at each site a car is injected with probability $1 - \beta$ (an outflow of a car from right end is obstructed by these cars). Its velocity is set to 0.

(3) Besides, we put cells at the sites $L + 2$, $L + 3$. At these two sites cars are always injected (this rule means that for cars at sites $-2, \ldots, L + 1$, there exist at least two preceding cars at any time). Its velocity is set to 0.

(4) We apply the updating rule of S-NFS to cars at sites $-2, \ldots, L + 1$. However, the slow-to-start effect (7) will apply only if $0 \leqslant x_i^{t-1}$ and $x_{i+S}^{t-1} \leqslant L - 1$.

(5) We remove all cars at -2, -1 and $L, \ldots, L + 3$ at the end of each time step.

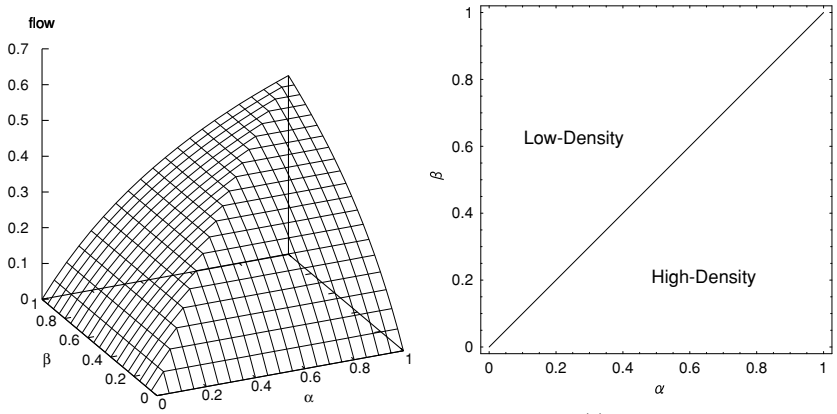

(*a*) flow-α-β diagram (*b*) α-β phase diagram

Figure 6. Definition of flow-α-β diagram of the ASEP ($p = 1.0$, $q = r = 0.0$) and a corresponding α–β phase diagram. The line of the first-order phase transition is given by $\alpha = \beta$.

These rules are devised in order to avoid an unnatural traffic jam caused by boundary conditions. Here, the rule (3) is needed in order that for cars at sites $-2, \ldots, L + 1$ there always exist at least two preceding cars. We need to apply S-NFS update rules to cars at sites L, $L + 1$ because otherwise the velocity of the car at site $L - 1$ is determined irrespective of the state at $L + 1$ even when $S = 2$.

With the use of this boundary condition, we can calculate flow-α-β diagrams (see figure 7) form which phase diagrams are derived (see figures 12). The phase diagram of the ASEP has been already known (see figure 6). In this diagram, the whole α–β region is divided into two phases in the case $p = 1.0$: low-density (LD) phase which is 'an α controlled phase'; and high-density (HD) phase which is 'a β controlled phase'. On the phase transition curve, the effect of α is balanced with that of β, and then these two phases coexist. The flow-α-β diagrams of the S-NFS model are considerably different form the result of the ASEP (see figure 7). The difference will be discussed in section 5. We restrict ourselves to the case $V_{\max} = 1$ and $p = 1.0$ in the following.

5. Phase transition curve

In this section, let us derive an analytic expression of the first-order phase transition curve of the S-NFS model by combining approximate flow-density relations at boundaries and fundamental diagrams. We extend the method proposed in papers [11, 12]. The method consists of three steps: first, we relate the flow and density near the boundaries of the system in OBC; next, in fundamental diagrams of PBC, we calculate the gradient of the free-flow line and jamming line; finally we can obtain phase diagrams for OBC from the above results.

5.1. Relation between flow and density near the boundaries

First, we calculate each flow J_l and J_r at the left or right end of this system. The configurations in figure 8 contribute flow at each boundary. Then with the use of the mean-field approach, the probability of the configuration (a) is $c_{(-1)}[1 - c_{(0)}]$. Similarly the probabilities of (b), (c) and (d) are $rc_{(-1)}c_{(0)}[1 - c_{(1)}]$, $c_{(L-1)}[1 - c_{(L)}]$, and $rc_{(L-1)}c_{(L)}[1 - c_{(L+1)}]$, respectively.

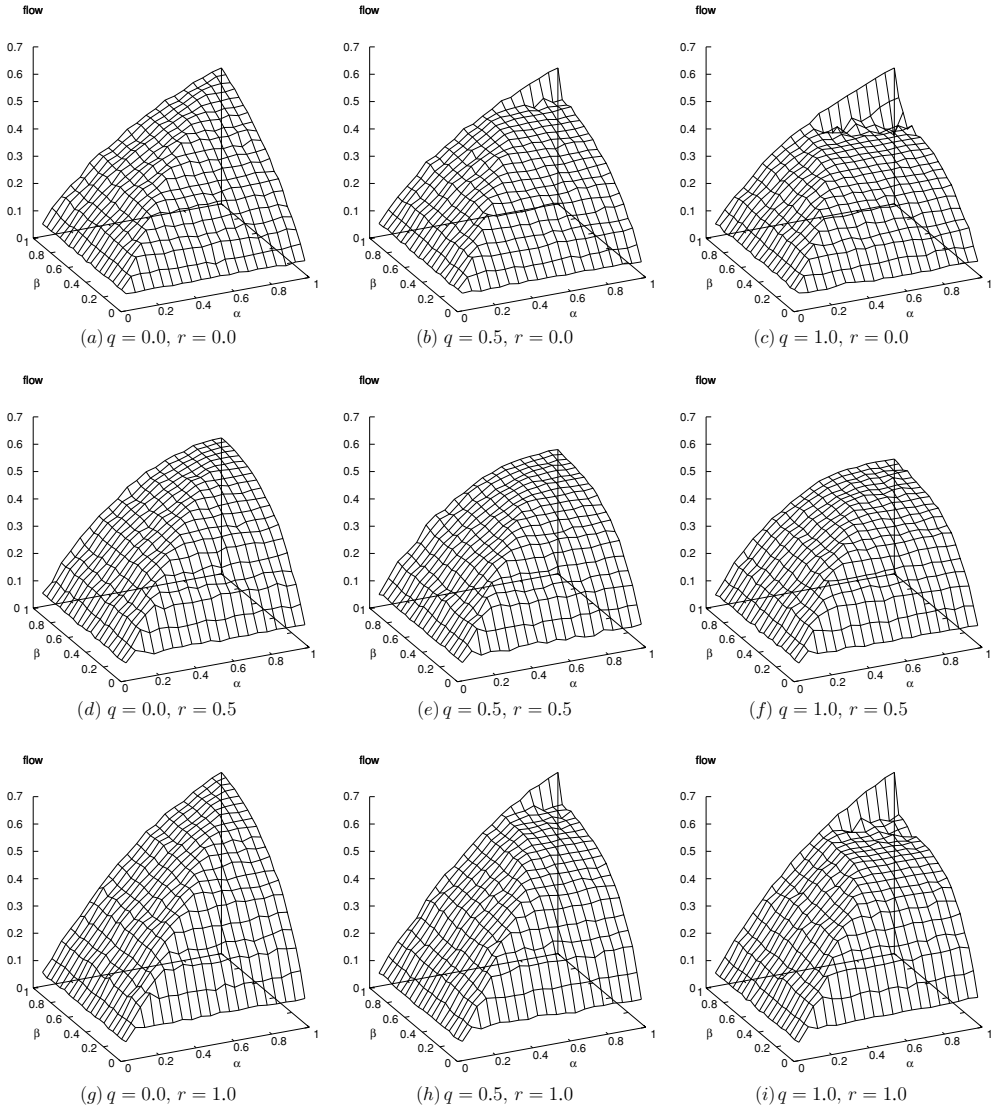

Figure 7. Flow-α-β diagrams of the S-NFS model with $p = 1.0$ and $V_{\max} = 1$. Note that flow suddenly rises near $\beta = 1.0$ in (b), (c), (h) and (i) because cars never take the slow-to-start mode even when $q \neq 0$.

Here, $c_{(j)}$ denotes the probability of finding a car at the site j. Because $c_{(-1)} = \alpha$ and $c_{(L)} = c_{(L+1)} = 1 - \beta$, we get

$$\begin{cases} J_l = \alpha(1 - c_{(0)})(1 + rc_{(0)}) \\ J_r = \beta[1 + r(1 - \beta)]c_{(L-1)} \end{cases} \tag{12}$$

where we assume $c_{(0)} = c_{(1)}$. Note that we ignored the possibility that a car at the site 0 cannot move by the slow-to-start effect in (b).

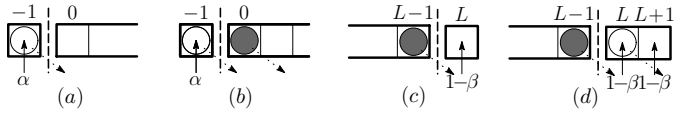

Figure 8. Configurations of cars contributing to flow at the left or right ends. Other configurations do not generate flow at both ends.

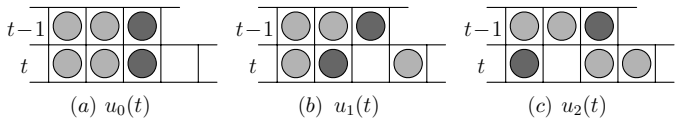

Figure 9. The connection between the parameter $u_g(t)$ and configurations of cars.

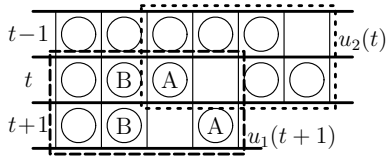

Figure 10. The case where $u_2(t)$ becomes $u_1(t+1)$.

5.2. *Approximate expression of fundamental diagrams*

Next we approximate the free-flow line and jamming line of PBC by straight lines as

$$\begin{cases} J_f = \rho = c_{(0)} & \text{(free-flow line)} \\ J_j = x(1-\rho) = x(1-c_{(L-1)}) & \text{(jamming line),} \end{cases} \tag{13}$$

where J_f and J_j denote the flow of free-flow and jamming phases, and x is a magnitude of the gradient of the jamming line. Here, we need to get the relations between x and q or r. The parameter x is related to the velocity of backward moving traffic clusters which we will calculate with the use of the mean-field approach.

Figure 9 shows the possible configurations at the right end of clusters. The symbols $u_g(t)$ $g \in \{0, 1, 2\}$ mean the probability of each configuration at time t. The subscript 'g' denotes the gradient of each configurations. For example, let us consider the probability that the configuration figure 9 (c) becomes (b) in the next time step, $u_2(t) \to u_1(t+1)$ (see figure 10). In order that (b) occurs, the slow-to-start effect is not active for the car A (the probability $1-q$). The car B does not move when (i) the driver's perspective is not active (the probability $1-r$) or (ii) although the driver's perspective is active, the car B still halts due to the slow-to-start effect (the probability qr). Thus we get the term $u_2(t)(1-q)(1-r+qr)$ which expresses the probability that $u_2(t)$ becomes $u_1(t+1)$. Considering other possibilities in the same way, we get the following recursion relations:

$$u_0(t+1) = u_1(t)q(1-r) + u_2(t)q \tag{14}$$

$$u_1(t+1) = u_0(t)(1-r) + u_1(t)(1-r+qr)(1-q+qr) + u_2(t)(1-q)(1-r+qr) \tag{15}$$

$$u_2(t+1) = u_0(t)r + u_1(t)r(1-q)(1-q+qr) + u_2(t)r(1-q)^2. \tag{16}$$

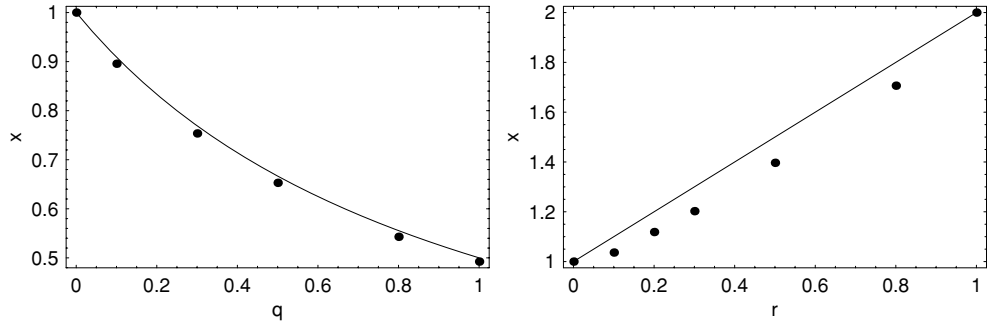

(*a*) x-q diagram ($r = 0.0$) (*b*) x-r diagram ($q = 0.0$)

Figure 11. The relation between the gradient of the jamming line x and probabilities q or r. The solid line denotes the approximate analytic result, and points denote the results of numerical simulations. There seem some discrepancies in (b). The reason is that we assume the shape of jamming line in the fundamental diagram to be straight although it is actually roundish.

We solve equations (14), (15) and (16) for the steady state $u_g(t+1) = u_g(t) = u_g$, and we get

$$u_0 = \frac{q[1 - r + (1 - q)r^2]}{1 - 2q^2r^2 + q(1 - r + r^2)} \tag{17}$$

$$u_1 = \frac{1 - (1 - q + q^2)r}{1 - 2q^2r^2 + q(1 - r + r^2)} \tag{18}$$

$$u_2 = \frac{[1 - q + q^2(1 - r)]r}{1 - 2q^2r^2 + q(1 - r + r^2)}. \tag{19}$$

Thus, we take the expectation $x = 0u_0 + 1u_1 + 2u_2$, and obtain the answer:

$$x = x(q, r) = \frac{1 + r - qr + q^2r - 2q^2r^2}{1 + q - qr + qr^2 - 2q^2r^2}. \tag{20}$$

The relations between x and q or r obtained from numerical simulations are plotted and compared with equation (20) in figure 11. The theoretical curve (20) gives a good estimation of numerical results.

5.3. Derivation of phase transition curve

Finally, we derive a phase transition curve for OBC from the above results. From (12) and (13), we obtain the following equations,

$$J_f = J_l \quad \Longrightarrow \quad c_{(0)} = \alpha[1 - c_{(0)}][1 + rc_{(0)}] \tag{21}$$

$$J_j = J_r \quad \Longrightarrow \quad x[1 - c_{(L-1)}] = \beta[1 + r(1 - \beta)]c_{(L-1)}, \tag{22}$$

which lead to

$$c_{(0)} = \frac{\alpha(r - 1) - 1 + \sqrt{\alpha^2(1 + 2r + r^2) + 2\alpha(1 - r) + 1}}{2r\alpha} \tag{23}$$

$$c_{(L-1)} = \frac{x}{\beta[1 + r(1 - \beta)] + x}. \tag{24}$$

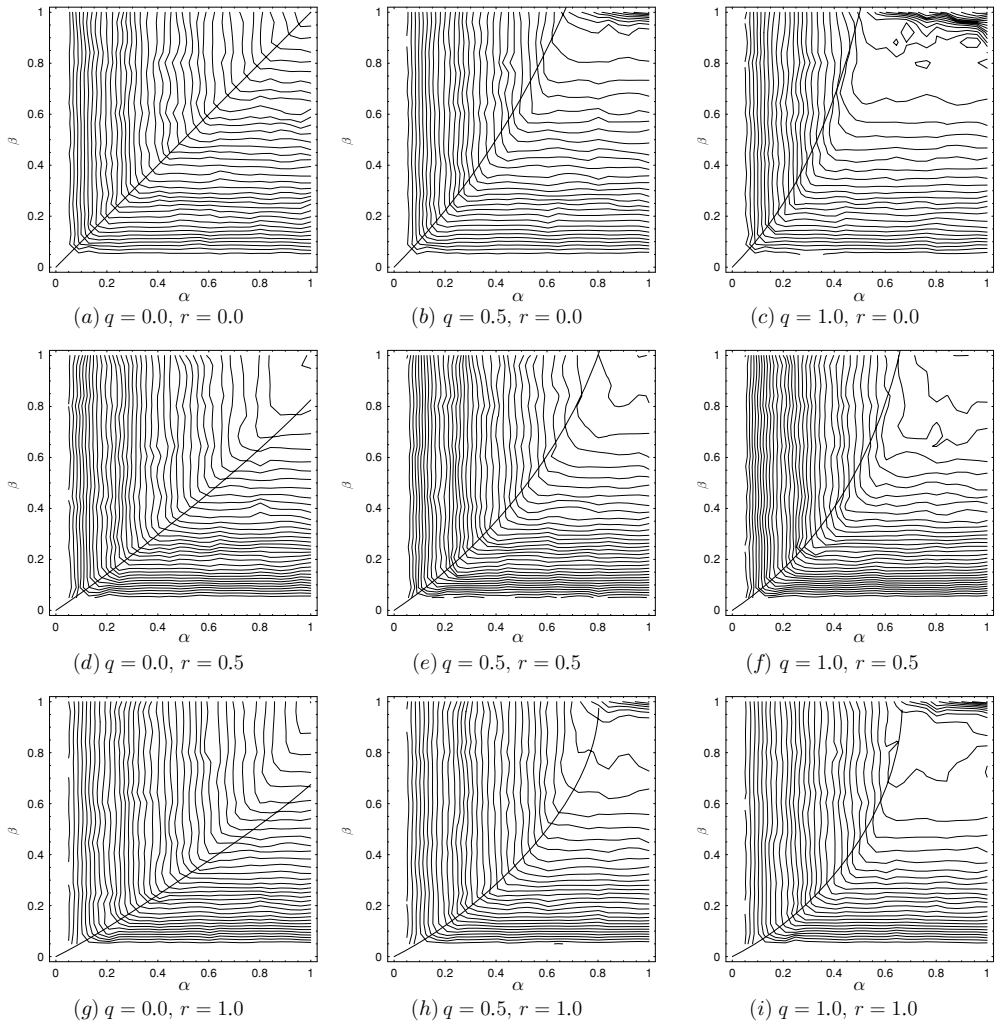

Figure 12. Approximate phase transition curves that are calculated by (25), and contour curves of flow-α-β diagram (figure 7). The theoretical curves are in good agreement with numerical results.

Using (13) and the equation $J_f = J_j$ which is the characteristic of two phase coexistence, we can get $c_{(0)} = x[1 - c_{(L-1)}]$. Substituting (24) into this equation, we can express β by q, r, x and α:

$$\beta = \frac{1+r}{2r} + \frac{\sqrt{[c_{(0)} - x]^2(1+r)^2 + 4rx[c_{(0)} - x]c_{(0)}}}{2r[c_{(0)} - x]} \tag{25}$$

where $c_{(0)}$ is written by α and r as in equation (23). This is the approximated curve of the phase boundary.

It should be noted that equations (23) and (25) are a singular when $r = 0.0$. Expression (25) becomes

$$\beta = \frac{x\alpha}{x(1+\alpha) - \alpha} \tag{26}$$

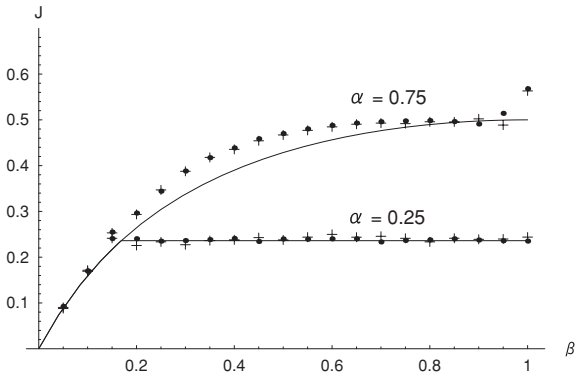

Figure 13. Flow is plotted against β at $\alpha = 0.25$ and $\alpha = 0.75$ when $p = q = r = 1.0$. The symbols + (•) represent data for $L = 600$ ($L = 3000$). Solid lines denote the approximate results (13) with (23), (24) and (25).

in this singular case. Figure 12 gives a comparison between the approximate phase transition curve (25) and contour curves of flow-α-β diagram obtained from numerical simulations. The phase transition curves are very close to those obtained from numerical simulations. However, we note that the shape of the jamming line in the fundamental diagram is assumed to be straight as (13). Therefore we see the approximate result is not good in the high flow region (where α and β are close to 1) for figure 12(d) because in this case the shape of the jamming line is apparently roundish (see figure 3(d)).

The phase diagram consists of LD and HD phases, but maximal-current (MC) phase does not appear. The driver's anticipation effect makes the area of the HD phase smaller whereas the slow-to-start effect gives the opposite tendency. The phase transition curve which is straight for the ASEP is bent downward by the driver's anticipation effect. However, if $q \neq 0$, the slow-to-start effect becomes dominant as flow increases.

The paper [12] also discusses a phase diagram of a model which includes only the slow-to-start effect. The structure of the phase diagram is similar to those of figure 12(c). The S-NFS model shows more variety of phase diagrams.

According to [12], for large β there appears the enhancement of the flow which looks like a MC phase. The enhancement is due to the finite system size effect and vanishes with increasing system size. Figure 13 demonstrates the effects of system sizes on our results. The shape of flow does not change with increasing system size. Since there does not appear a plateau at $\alpha = 0.75$, we judge that the MC phase does not exist when $p = 1.0$ for the S-NFS model.

6. Summary and conclusions

In this paper, we have considered a stochastic extension of a traffic cellular automaton model recently proposed by one of the authors [7]. This model (which we call the S-NFS model) contains three parameters which control random braking, slow-to-start and driver's perspective effects. With special choice of these parameters, the S-NFS model is reduced to previously known traffic CA models such as the NS model, QS model, SlS model etc. Hence the S-NFS model can be considered as a unified model of these previously known models. Next, we investigated fundamental diagrams of the S-NFS model. The shape of a fundamental diagram

of the S-NFS model is similar to that with use of empirical data. Especially, the metastable branches, which are indispensable to reproduce empirical fundamental diagrams, clearly seen even when stochastic effects are present. This robustness of metastable branches in this model is advantageous because empirical data show metastability even though stochastic effects always exist in real traffic. Thus we can expect that the S-NFS model captures the essential feature of empirical traffic flow and is very useful for investigating various traffic phenomena such as jamming phase transition as well as for application in traffic engineering. Finally, we investigated phase diagrams of the S-NFS model with $V_{\max} = 1$ and $p = 1.0$. The analytic expression of the phase transition curve is obtained from the approximate relations between flow and density near the boundary, together with the approximate gradient of jamming lines in fundamental diagrams. The analytic phase transition curve successfully explains those of numerical simulations. Recently we have found that, in the case $p < 1.0$, the MC phase appears in the the S-NFS model. The analysis in the cases $V_{\max} > 1$ or $p < 1.0$ will be reported elsewhere [20].

Acknowledgments

The authors thank the Japan Highway Public Corporation for providing us with the observed data. A part of this work is financially supported by a grant-in-aid from the Ministry of Education, Culture, Sports, Science and Technology, Japan (no 18560053).

References

[1] Chowdhury D, Santen L and Schadschneider A 2000 *Phys. Rep.* **329** 199
[2] Nagel K and Schreckenberg M 1992 *J. Physique* I **2** 2221
[3] Takayasu M and Takayasu H 1993 *Fractals* **1** 860
[4] Barlovic R, Santen L, Schadschneider A and Schreckenberg M 1998 *Eur Phys. J.* B **5** 793
[5] Fukui M and Ishimashi Y 1996 *J. Phys. Soc. Japan* **65** 1868
[6] Nishinari K and Takahashi D 2000 *J. Phys. A: Math. Gen.* **33** 7709
[7] Nishinari K, Fukui M and Schadschneider A 2004 *J. Phys. A: Math. Gen.* **37** 3101
[8] Kanai M, Nishinari K and Tokihiro T 2005 *Phys. Rev.* E **72** 035102
[9] Schadschneider A and Schreckenberg M 1998 *J. Phys. A: Math. Gen.* **31** L225
[10] Rajewsky N, Santen L, Schadschneider A and Schreckenberg M 1998 *J. Stat. Phys.* **92** 151
[11] Kolomeisky A B, Schütz G M, Kolomeisky E B and Straley J P 1998 *J. Phys. A: Math. Gen.* **31** 6911
[12] Appert C and Santen L 2001 *Phys. Rev. Lett.* **86** 2498
[13] Ishibashi Y and Fukui M 2002 *J. Phys. Soc. Japan* **71** 2335
[14] Sugiyama Y and Nakayama A 2003 *Interface and Transport Dynamics* ed H Emmerich, B Nestler and M Schreckenberg (Berlin: Springer) p 406
[15] Ishibashi Y and Fukui M 1996 *J. Phys. Soc. Japan* **65** 2793
[16] Jiang R, Wu Q S and Wang B H 2002 *Phys. Rev.* E **66** 036104
Huang D W and Huang W N 2003 **67** 068101
Jiang R, Wu Q S and Wang B H 2003 **67** 068102
[17] Huang D W 2005 *Phys. Rev.* E **72** 016102
[18] Wolfram S 1986 *Theory and Applications of Cellular Automata* (Singapore: World Scientific)
[19] Kerner B S and Klenov S L 2002 *J. Phys. A: Math. Gen.* **35** L31
[20] Sakai S, Nishinari K and Iida S in preparation